J. Fluid Mech. (1990), *vol.* 215, *pp.* 481–502
Printed in Great Britain

Flow and transport in single rock fractures

By K. MURALIDHAR
Department of Mechanical Engineering, Indian Institute of Technology, Kanpur 208016, India

(Received 1 March 1989)

The present work is a numerical study of fluid flow and energy transport in single rock fractures. Each fracture is modelled as a parallel channel with a distribution of contact areas where the fracture aperture is zero. The pressure drop required to sustain a given rate of flow is calculated by solving the Stokes equations along with the incompressibility constraint. The permeability of the fracture is then determined as the ratio of mean flow and pressure drop. With flow distribution known, the advection–diffusion equation is solved for a thermal mixing problem. All differential equations have been solved by the finite-element technique.

Results show that the fracture permeability is affected by the presence of contact areas and the magnitude of h, the mean fracture aperture. The limiting case of zero aperture is realized at $h/L \leqslant 0.016$, where L is the characteristic dimension of the fracture. The other limiting case of a two-dimensional fracture is seen for $h/L \geqslant 1$. The thermal dispersion profiles at steady state are unaffected by the size of aperture h and the presence of contact areas for Péclet numbers Pe less than 50 and a contact fraction of up to 20%. However, the transient dispersion problem is seen to be influenced by the contact areas for $Pe > 10$.

1. Introduction

Fluid flow and heat transfer in fractured rocks and geologic faults are rather poorly understood. It appears that fluid movement falls into distinct regimes, each of which is governed by capillary theory, Darcy's law and cubic law, respectively. The controlling features which determine pressure drop are fluid saturation and fracture aperture. Saturation is defined as the ratio of the volume of water present in a fracture to the volume of the fracture opening. A capillary theory for unsaturated flow in a fractured matrix has now been developed by Wang & Narasimhan (1985). In the present study, a water-saturated single rock fracture has been considered. The flow pattern through this fracture and the details of thermal dispersion have been numerically determined by solving the appropriate differential equations. The detailed knowledge of thermohydraulic behaviour of a single fracture is expected to assist fracture network models which characterize a rock as a whole. With plans to dispose of nuclear waste from power plants in granitic rock formations under the earth, such characterization has immense practical value (Chapman & McKinley 1987). Fluid movement in this application refers to groundwater flow and heat transfer relates to energy release by radioactive decay.

The conventional approach to studying flow in saturated fractures involves modelling them as parallel plates with a spacing h, which is a spatial variable. The average fracture aperture is determined by one of the following methods.

(i) h = Flow volume within fracture/area of fracture plane.

(ii) $$h = \frac{1}{N}\sum_{i=1}^{N} h_i,$$

where h_i are individual apertures measured at N points in the fracture. In many laboratory experiments it is easy to measure the volume-averaged aperture rather than its distribution over the fracture plane. Sample values of h_i can then be generated by a random statistical process which preserves this average. The fracture aperture h which governs pressure drop is determined from h_i using weighting functions that are biased towards the small apertures. This method produces an equivalent aperture smaller than the laboratory average. The fracture permeability is calculated from the 'cubic law' (Snow 1968)

$$K = \frac{h^2}{12}. \tag{1}$$

The momentum equation in this approach is assumed to be Darcy's law (Bear 1972) which connects mean velocity u to the regional pressure gradient $\mathrm{d}p/\mathrm{d}x$ as

$$u = -\frac{K}{\mu}\frac{\mathrm{d}p}{\mathrm{d}x}, \tag{2}$$

where μ is fluid viscosity. Regions of the fracture where the local aperture is zero are called 'contact areas', and fluid has to turn around such regions away from the direction of the mean pressure gradient. The two definitions of fracture aperture h given above are inaccurate if the fracture has a distribution of contact areas and are useful only in relatively open fractures. Tsang (1984) has extended the cubic law to include effects of tortuosity of flow path arising from contact areas. Empirical tortuosity factors have also been used by Walsh & Brace (1984) in their work on porosity and permeability of rocks subjected to external pressure. Brown (1987) has studied flow in fractures whose apertures are generated using fractal theory, with flow governed by the Reynolds equation of lubrication,

$$\nabla \cdot h^3 \nabla p = 0, \tag{3a}$$

$$h = h(x, y), \tag{3b}$$

and

$$\boldsymbol{u} = \frac{h^2}{12\mu}\nabla p. \tag{3c}$$

The average aperture is computed from (3c) interpreted in terms of an average velocity and pressure drop.

With the velocity field determined by one of the methods given above, the spreading of thermal wakes, either from isolated heat sources or due to mixing of a hot and a cold stream is calculated from the following advection–diffusion equation (Kays & Crawford 1980):

$$\frac{\partial T}{\partial t} + \boldsymbol{u}\cdot\nabla T = \alpha \nabla^2 T. \tag{4a}$$

In this equation, T is temperature, t is time and α is the thermal diffusivity of the fluid. Since the velocity field $\boldsymbol{u}$ in (4a) is based on an empirical description of the flow,

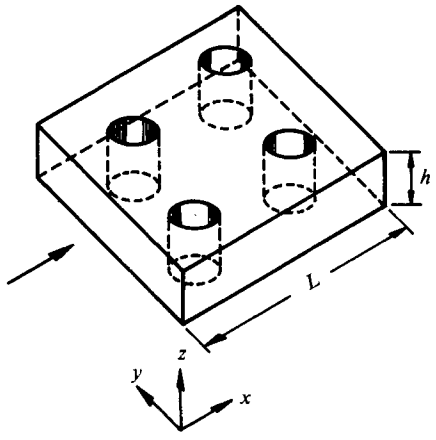

FIGURE 1. Model of a rock fracture with contact areas.

it ignores tortuosity and this equation frequently under-predicts the spreading of wakes. For this reason, (4*a*) is modified to the form

$$\frac{\partial T}{\partial t} + \boldsymbol{u} \cdot \nabla T = (\alpha + \bar{\alpha}) \nabla^2 T, \tag{4b}$$

where $\bar{\alpha}$ is the dispersion coefficient. Developments in the theory of solute transport, analogous to energy transport, have been summarized by Dagan (1987) for flow in a porous medium and details of the calculation of $\bar{\alpha}$ may be found in that reference.

The objectives of the present study are the following. First the fracture permeability defined as the ratio of mean flow and pressure drop across the length of the fracture is calculated using Stokes equations. These equations hold for a slow moving Newtonian fluid (Schlichting 1979). They are solved numerically in the complex pore space of the fracture. Secondly, the transport equation is solved using the velocity field $\boldsymbol{u}$ obtained from the Stokes equations. The changes in permeability and the temperature profiles for different values of the percentage contact area and aperture have been determined in detail in this work.

The rock fracture has been modelled in this work as consisting of parallel planes with a distribution of contact areas. This is shown in figure 1. It is assumed that the variation of aperture between contact areas is unimportant, as far as the pressure drop/dispersion problem is concerned. This implicitly states that contact areas are the primary cause of differences between fractures modelled as parallel plates and laboratory experiments. This is not universally true. For example, open fractures with little contact area will still suffer substantial pressure drop due to variable aperture. However, such fractures are easily analysed by one of the conventional methods given earlier. One reason for the choice of the contact area to describe a fracture is because of its easy measurability (Pyrak-Nolte *et al.* 1987). The parallel-plate model of a fracture with a distribution of circular contact areas is equivalent to the idealization of soil as a homogeneous, isotropic porous medium.

The contact areas are assumed to be circular in shape in this study. This is not of serious concern since our numerical experiments show that the fracture permeability is only weakly dependent on the shape of contacts, for a large contact area. Permeability is defined as the ratio of mean flow through the fracture and the accompanying pressure drop. This is further normalized by the permeability of a

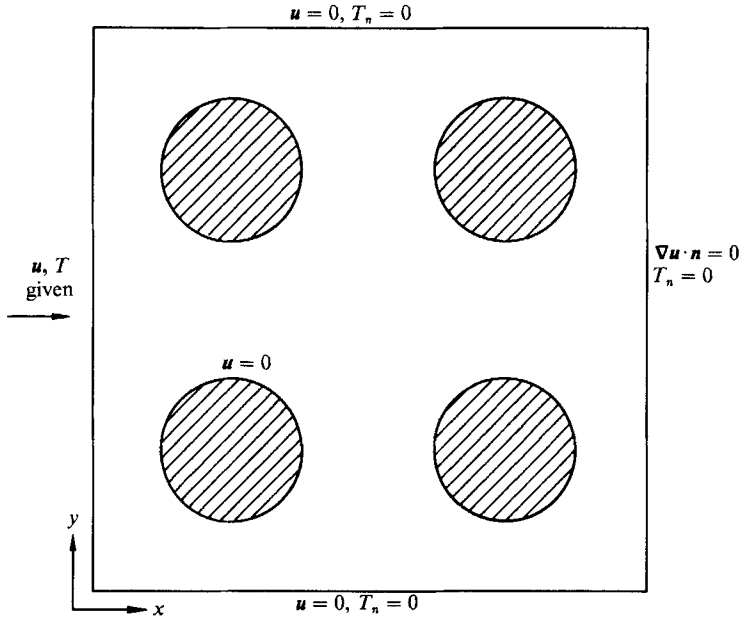

FIGURE 2. Fracture plane and coordinate system.

fracture with no contact area. The normalized permeability has been called equivalent permeability in this study and given the symbol K. Results are presented for K as a function of the contact area. A similar study has been reported by Coulaud, Morel & Caltagirone (1988), who model flow in porous media as flow past closely spaced cylinders.

The thermal problem consists of steady and unsteady mixing of two parallel streams at different temperatures. The flow and transport equations have been solved here by a Galerkin finite-element technique.

2. Formulation

Figure 2 shows a section of the fracture with several contact areas. The Cartesian coordinate system and the direction of flow are also shown in this figure. The formulation is presented here in dimensionless form. Let u_m, the mean velocity in the fracture be a velocity scale and d, typically the size of a contact area be the lengthscale. The full equations governing fluid flow and heat transfer in the open spaces of the fracture are the Navier–Stokes equations,

$$\boldsymbol{u}_t + \boldsymbol{u}\cdot\nabla\boldsymbol{u} = \frac{1}{Re}\nabla^2\boldsymbol{u} - \nabla p, \tag{5}$$

the incompressibility constraint,

$$\nabla\cdot\boldsymbol{u} = 0 \tag{6}$$

and the advection–diffusion equation,

$$T_t + \boldsymbol{u}\cdot\nabla T = \frac{1}{Pe}\nabla^2 T. \tag{7}$$

In (5), $Re = u_m d/\nu$ is the Reynolds number, ν is the kinematic viscosity of the fluid, and Pe is the Péclet number, $u_m d/\alpha$. Since u_m, the characteristic velocity of groundwater motion is quite small, Re is also expected to be small. For example, the groundwater velocity used in nuclear waste disposal design is 100 m/year. For an average fracture opening of 0.5 mm, such as in crystalline rock, the Reynolds number is 0.002. Under these circumstances, it can be assumed that $\boldsymbol{u}\cdot\nabla\boldsymbol{u}$, the inertial terms are uniformly small, and hence can be dropped from (5) (Schlichting 1979). Further, the fracture aperture is also a small quantity in relation to its length, i.e. $h/L \ll 1$, where L is a linear fracture dimension. Since the velocity component w, normal to the fracture plane scales as

$$\frac{w}{u_m} = O\left(\frac{h}{L}\right), \tag{8}$$

we assume that w is identically zero in the fracture. This is equivalent to saying that the pressure is uniform over the fracture aperture. With these simplifications, the flow equations (5) and (6) reduce to the following form:

$$u_t - \frac{1}{Re}(u_{xx}+u_{yy}+u_{zz}) = -p_x, \tag{9a}$$

$$v_t - \frac{1}{Re}(v_{xx}+v_{yy}+v_{zz}) = -p_y, \tag{9b}$$

$$u_x + v_y = 0. \tag{9c}$$

To eliminate the z-coordinate in (9), these are depth-averaged over the fracture aperture. It is necessary at this point to assume a suitable profile for $\boldsymbol{u}$ as a function of z. The form

$$\boldsymbol{u} = \bar{\boldsymbol{u}}(x,y)\,g(z), \tag{10}$$

where

$$g(z) = \frac{6z(h-z)}{h^2}, \quad \frac{h}{L}\to 0,$$

guarantees the no-slip condition at $z = 0$ and $z = h$ and a non-zero value for $\boldsymbol{u}$ between $z = 0$ and h. The parabolic profile for g is a natural choice since it conforms to the fully developed shape of a velocity profile between two walls. Equation (10) is applied everywhere in the fracture and so this procedure is equivalent to assuming zero development length for the flow. Equation (10) is not a point-wise solution of (9). However, it is useful to construct depth-averaged solutions in the fracture.

Substituting (10) in (9) and integrating them as $\int_0^h dz$ leads to

$$\bar{u}_t - \frac{1}{Re}\left(\bar{u}_{xx}+\bar{u}_{yy}-\frac{12\bar{u}}{h^2}\right) = -p_x, \tag{11a}$$

$$\bar{v}_t - \frac{1}{Re}\left(\bar{v}_{xx}+\bar{v}_{yy}-\frac{12\bar{v}}{h^2}\right) = -p_y, \tag{11b}$$

$$\bar{u}_x + \bar{v}_y = 0. \tag{11c}$$

It is assumed that the temperature is uniform across the fracture aperture. This yields the depth-averaged advection–diffusion equation

$$T_t + \bar{\boldsymbol{u}}\cdot\nabla T = \frac{1}{Pe}(T_{xx}+T_{yy}), \tag{12}$$

assuming that the bounding rock surfaces which define the fracture geometry have a low thermal conductivity. The process of depth-averaging the temperature distribution eliminates the possibility of Taylor dispersion due to shear in the flow. This is not expected to cause errors in the transverse dispersion problem studied here. Taylor dispersion due to shear in the velocity profile in the z-direction (equation (10)) will change the dispersion coefficient from α to $\alpha + uh$ in dimensional variables and $1/Pe$ to $(1/Pe + h/L)$ in dimensionless variables. Clearly Taylor dispersion can be ignored if $\alpha \gg uh$ or $1/Pe \gg h/L$. Consider the following commonly used numbers in fracture hydrology: $\alpha(\text{water}) = 16 \times 10^{-8}$ m^2/s, $u = 100$ m/year, $h = 0.5$ mm. Then $uh = 16 \times 10^{-10}$ m^2/s and $\alpha \gg uh$.

Initial conditions required to start the transient calculation correspond to a stationary, cold fluid, i.e. $\boldsymbol{u} = 0$ and $T = 0$ at $t = 0$. As discussed later in this paper, velocity transients last only for a short duration and hence may be ignored. In the discussion given below, $\boldsymbol{u}$ refers to the velocity field at steady state, obtained by setting $\boldsymbol{u}_t = 0$ in (11).

Equations (11) and (12) are solved subject to the following boundary conditions:

$$\left.\begin{aligned} &\bar{\boldsymbol{u}} \text{ prescribed on the inflow boundary,} \\ &\nabla \bar{\boldsymbol{u}} \cdot \boldsymbol{n} = 0 \text{ on the outflow boundary,} \\ &\bar{\boldsymbol{u}} = 0 \text{ on the sidewalls} \quad (y = 0, L) \\ \text{or} \quad &\frac{\partial \bar{u}}{\partial y} = \bar{v} = 0 \text{ on the sidewalls.} \end{aligned}\right\} \tag{13}$$

On the inflow plane, $\bar{u}$ is taken as a constant and $\bar{v}$ as zero. Calculations reveal that any other distribution at $x = 0$ (say, parabolic) has only a small influence on the magnitude of equivalent permeability. Studies with both the no-slip and symmetry conditions applied on the sidewalls $y = 0$ and $y = L$ are reported here. The exit boundary condition is unknown at the beginning of a calculation. The gradient condition implied by (13) has the advantage that it is the least reflective of all possible choices (Peyret & Taylor 1980), i.e. is known to affect the interior solution the least. Pressure need be specified at only one point in the flow domain, for determinacy. This point has been chosen to be on the exit plane ($x = L$). The temperature boundary conditions for transverse dispersion are

$$\left.\begin{aligned} T &= 0, \quad x = 0, \quad y > \tfrac{1}{2}L \\ &= 1, \quad x = 0, \quad y < \tfrac{1}{2}L \\ &= 0.5, \quad x = 0, \quad y = \tfrac{1}{2}L, \\ T_y &= 0, \quad y = 0, L, \quad T_x = 0, \quad x = L. \end{aligned}\right\} \tag{14}$$

The sidewalls at $y = 0$ and L in (14) can be interpreted either as insulating or as being symmetry planes. On all contact areas, we specify the no-slip, non-conducting conditions

$$\bar{\boldsymbol{u}} = 0, \quad \nabla T \cdot \boldsymbol{n} = 0. \tag{15}$$

Equations (11) are solved simultaneously to extract a velocity and pressure field. The average pressure drop across the fracture is computed by integrating the pressure difference using Simpson's rule. Equivalent permeability K is then obtained as the ratio (average velocity)/(average pressure drop), normalized by this value for no contact area. With this normalization, K becomes independent of Re, the

Reynolds number at the Stokes limit $Re < 1$. Once the velocity field is known, it is possible to solve for temperature from (12).

2.1. *Special cases*

It can be seen that the transport equation is independent of h, the aperture. However, h is a parameter in the flow equations and hence K depends on the choice of h relative to the fracture field dimension L. The following two special cases arise as h approaches either zero or infinity.

$h \to 0$

For small values of h, (11) reduce to the form

$$\bar{\boldsymbol{u}} = -\tfrac{1}{12}h^2 \nabla p Re$$

and

$$\nabla \cdot \bar{\boldsymbol{u}} = 0,$$

the Darcy equations.

When h is a spatial variable, the continuity equation is of the form

$$\nabla \cdot \boldsymbol{u}h = 0$$

so that the equation governing p is

$$\nabla \cdot h^3 \nabla p = 0,$$

identical to the lubrication equation, (4a). Hence, when $h \to 0$, the viscous pressure drop due to the proximity of the bounding walls ($z = 0$ and h) is predominant. The tortuosity effects due to flow moving around contact areas are accounted for by the terms $(\bar{u}_{xx} + \bar{u}_{yy})$ in the Stokes equations. These are of secondary importance when $h \to 0$. The boundary conditions at $y = 0$ and L applied to the governing equations at the limit $h \to 0$ make the problem mathematically ill-posed. To circumvent this difficulty, the Darcian problem is solved by the Stokes solver without the no-slip conditions on the sidewalls $y = 0$ and L.

$h \to \infty$

For large values of h, one recovers two-dimensional fluid flow governed by the equations

$$\bar{u}_{xx} + \bar{u}_{yy} = Re \nabla^2 p,$$

$$\nabla \cdot \bar{\boldsymbol{u}} = 0.$$

This limit is sometimes realized in geologic faults (e.g. Ghost Dance fault at Yucca Mountains, Nevada, USA; see Montazer & Wilson 1984). It can be expected that, at this limit, the effect of contact areas is strongly felt, and the deviation between Darcy and Stokes models would be the greatest. It is also possible that inertial effects are not entirely negligible in this problem. However, the emphasis of this paper is not on fractures or faults of large aperture, but in rock fractures with a small aperture whose permeability is affected by contact areas.

3. Method of solution

Equations (11) and (12) subject to boundary conditions (13)–(15) have been solved by a Galerkin finite-element method (Baker 1983). The discrete elements which subdivide the flow domain are chosen as triangular. Velocity and temperature are interpolated at six modes and pressure at three nodes. This is called unequal-order

interpolation, and is equivalent to the use of a staggered mesh in finite-difference schemes (Patankar 1980). It is related to the difference in the highest derivatives of velocity and pressure, as they appear in the governing equations. The elements are chosen as isoparametric and this allows an exact representation of circular boundaries such as the contact areas. Equations (11) are simultaneously solved by assembling the finite-element equations into a global matrix. The system of algebraic equations has been inverted by a sparse matrix solver (Duff 1980). This is followed by the solution of the transport equation. Unsteady problems are treated by an implicit finite-difference procedure, resulting in a marching solution along the time axis. For the level of discretization used in this study, no upwind approximation was found necessary for the convective terms in the transport equation for Péclet number up to 10, and in some cases, up to 100.

In the results reported here, the grid is so chosen that the smallest obstacle is resolved by 16 nodal points for velocity and temperature, and 8 nodal points for pressure. Selected runs with nodal points increased by a factor of four showed a change in equivalent permeability and exit temperature profiles of less than 4%. A time step $\Delta t = 0.1$ has been found satisfactory in all unsteady calculations.

3.1. *Code validation*

A description of validation of the computer codes used in the present study is included in the Appendix.

4. Results

Results are presented below for a parallel channel with aperture h, a region size of $L = 6$ units and a distribution of contact areas. Each length unit is approximately the size of the contact area. The contact areas are taken as circular in shape, and arranged in a reasonably uniform pattern. The permeability of a fracture with a given h depends primarily on the total percentage contact area; their shape size and distribution play only a secondary role. One can think of certain extreme patterns of distribution where K goes to zero, even for a small percentage contact area. The probability of occurrence of such patterns in a real fracture is expected to be small. The choice of L as six units is arbitrary and does not alter the results, since K is only a function of percentage contact.

4.1. *Steady flow in a fracture*

Figure 3 is a plot of K, the equivalent permeability, as a function of N, the number of contact areas. Each contact occupies an area of 2.18% over the fracture. The largest value of N studied here is 9, which corresponds to 20% of the fracture. The dependence of K on N has been plotted for three cases corresponding to the aperture $h = \infty$, the two-dimensional problem; $h \to 0$, the Darcy limit; and $h = 1$, an intermediate value. In each problem K monotonically decreases with increasing contact area. The decrease is, however, rapid in the two-dimensional problem since the tortuosity of flow path alone contributes to the pressure drop. At the Darcy limit ($h \to 0$), K diminishes gradually for increasing N, since much of the pressure drop occurs owing to the proximity of the bounding walls of the fracture in the z-direction. At $h = 1$, (relative to $L = 6$) pressure drops due to both tortuosity and wall friction are operative. An empirical method of calculating equivalent permeability is to obtain h based on the real flow volume available in the fracture. For a contact area

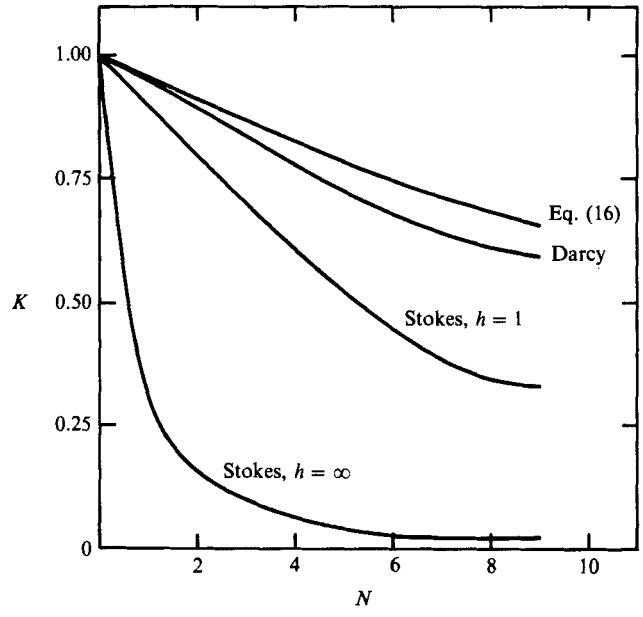

FIGURE 3. Plot of equivalent permeability as a function of the number of contact areas.

fraction equal to C, the flow volume is $(1-C)L^2$; the aperture of a uniform open fracture of edge L with this volume is

$$h = (1-C)L^2/L^2 = 1-C,$$

and hence, from (1), the equivalent permeability

$$K = (1-C)^2. \tag{16}$$

This result is also plotted in figure 3. Values predicted by (16) are quite close to the Darcy permeabilities.

For the special case of $N = 9$ ($\sim 20\%$ contact), figure 4 shows the variation in equivalent permeability with respect to the fracture aperture h. The two limits of $h \to 0$ and $h \to \infty$ are also shown in the figure. It is seen from here that for h/L of order unity or greater, the two-dimensional approximation is valid. It must be noted here that real fractures are slender and if L is interpreted as the real length dimension, h/L would always be quite small. It is implied in this work that L^2 is a measure of a repeating (or at least a representative) area of the fracture, and that L is much smaller than the entire linear dimension of the fracture. Taking this into account, fractures with $h/L \geqslant 1$ are still seldom observed in rocks.

The Darcy limit is reached at $h/L \leqslant 0.016$. Fractures which satisfy this criterion are thin. These are affected by the contact area, though they are insensitive to both their pattern of distribution and degree of fineness. Further results for $h = 1$ and $h \to \infty$ are given below.

The total pressure drop required to sustain a given quantity of flow in a fracture consists of contributions from viscous friction at the bounding planes ($z = 0$ and h) and the contact areas. The no-slip condition used in the present study at the sidewalls ($y = 0, L$) causes additional pressure drop. To ensure that the permeability results are insensitive to the sidewall boundary conditions, calculations have been repeated with symmetry boundary conditions applied at $y = 0$ and L. The results of these

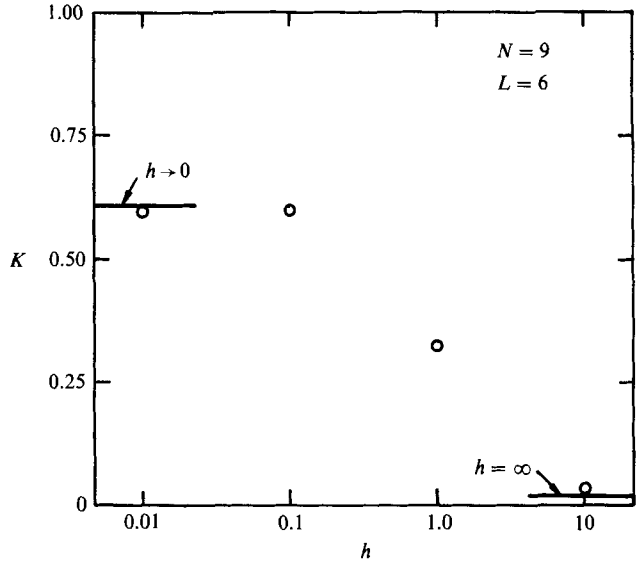

FIGURE 4. Plot of equivalent permeability as a function of fracture aperture.

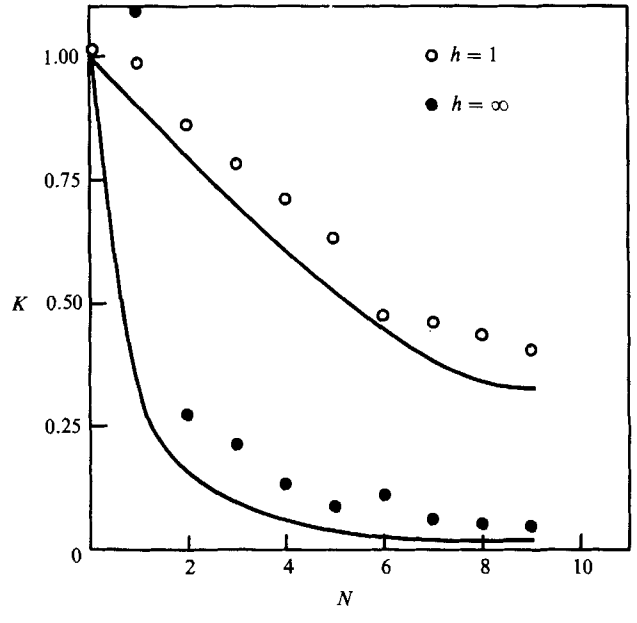

FIGURE 5. Plot of equivalent permeability as a function of the number of contact areas: symmetric sidewalls.

calculations are shown in figure 5 for $h = 1$ and $h = \infty$. The equivalent permeability K has been normalized with its value at zero contact area ($N = 0$), but with no-slip conditions at the sidewalls. Hence, the magnitudes of K in figures 3 and 5 are directly comparable. The Stokes solutions from figure 3 have been included here for comparison. It is seen from these figures that the permeability calculated using symmetry conditions is always larger than that calculated with no-slip conditions at $y = 0$ and L. This difference is large when contact area is small and h is large. For

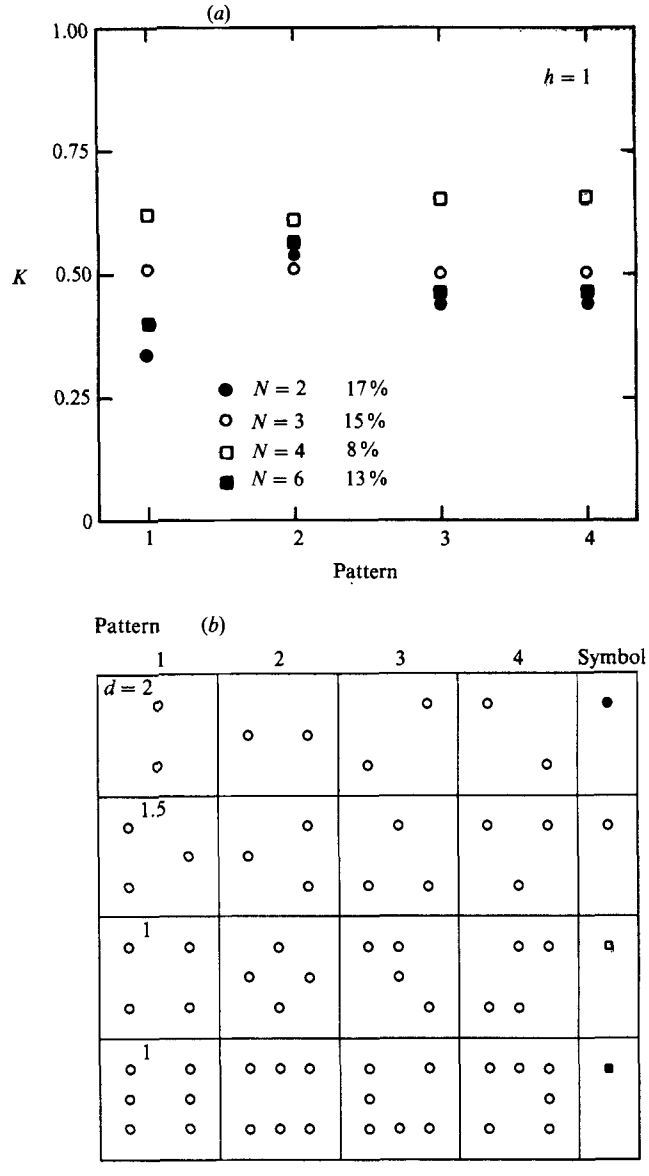

FIGURE 6. (*a*) Plot of variability of equivalent permeability with pattern of distribution of contact areas. (*b*) Patterns of contact areas used in (*a*).

$N > 4$ (contact area > 9%), these boundary conditions are secondary at any value of h. Results with the no-slip condition alone are presented below.

Figure 6(*a*) shows the variability in equivalent permeability with the pattern of distribution of contact area. Four different patterns involving circular contact areas have been considered for four different values of N. These patterns are summarized in figure 6(*b*). These studies have been performed for various values of h. Results show that the variability of K with pattern is large for large values of h and small contact area. For a given percentage contact, K is largest for those patterns which permit the formation of large pathways to flow. These are called 'channels', in the porous-media literature. With the exception of patterns which form such channels

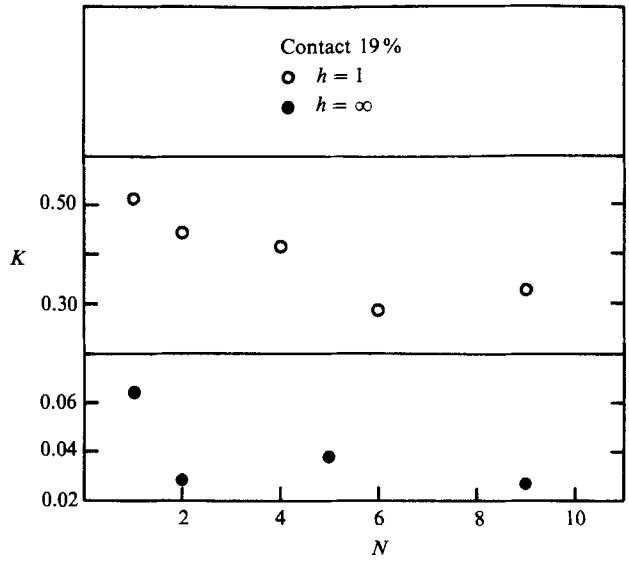

FIGURE 7. Variation of equivalent permeability with fineness of contact areas.

(for example, $N = 2$, pattern 2; $N = 6$; pattern 2), the variability of K with the location of contact areas is usually small. It further decreases with increasing fineness of contact and increasing contact area.

Figure 7 shows the dependence of K on the fineness of distribution of contact, keeping the total contact area a constant. Increasing fineness is accomplished by subdividing a large circular area into smaller circular areas, the number of such areas representing the extent of fineness. The trend seen in figure 7 is towards lower permeability for increasing fineness of distribution. However, beyond a certain fineness level K is nearly constant, with some fluctuation arising from differences in pattern of location of contact areas. Such a procedure of starting with a large single contact area and studying the permeability of the fracture as it is subdivided, keeping the total contact area a constant, is useful in determining the permeability of rock fractures with a known percentage contact. Real fractures have a degree of fineness which is much larger than what can be simulated numerically on a main frame computer (for example, VAX 11/780). The above procedure is a realistic alternative to modelling these fractures directly.

4.2. *Transport in fractures*

Once the velocity field is computed, it is then possible to solve the transport problem (equation (12)) for dispersion patterns of energy. The solution depends on the choice of initial and boundary conditions for temperature. For unsteady problems, the fluid in the fracture is taken to be at zero temperature, with thermal loading arising at the inflow boundary. To bring into focus the dispersion problem, i.e. the spreading of thermal wakes, we consider the boundary condition given by (14). This corresponds to two streams at different temperature ($T = 1$ and 0) which start to mix in the fracture. Mixing is initiated at their interface, and the dispersion problem consists of determining the width of the mixing region. A situation such as this is encountered when two fractures containing fluids at different temperatures feed into a third one.

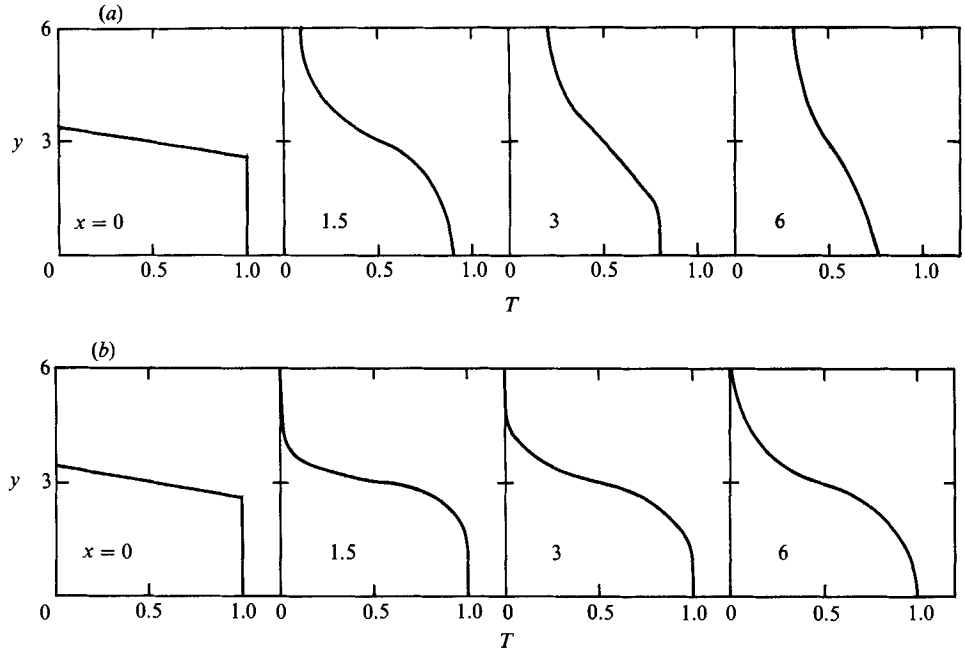

FIGURE 8. Development of temperature profiles with distance at steady state with no contact area: (*a*) $Pe = 1$; (*b*) $Pe = 10$.

4.2.1. *Steady state*

Transport of thermal energy at steady state is considered first. Figure 8(*a*, *b*) shows development of temperature profiles in a parallel channel with no contact area. Results for two Péclet numbers (1 and 10) are presented. The temperature profiles at various x-positions given in figure 8(*a*) at $Pe = 1$, correspond closely to the conduction limit ($Pe = 0$). Hence, the conduction regime may be thought of as extending up to $Pe \approx 1$. At this limit, the temperature difference between the hot and cold streams diminishes rapidly with distance. At higher Péclet numbers this difference persists over larger distances in the downstream direction. These results are independent of the aperture h. The flow is nearly parallel everywhere, except near the sidewalls $y = 0$ and L, where a no-slip condition is applied. An exception occurs at the Darcy limit ($h \to 0$), when the mathematical character of the flow equations (9) changes, and the no-slip conditions on the sidewalls can no longer be applied. Though the near-wall velocity field is altered at the Darcy limit, the overall temperature profiles remains unaffected. The differences arising from changing the fracture aperture become truly negligible if the Péclet number is larger than 10.

Figure 9 shows an explicit comparison of temperature profiles using the Darcy and the Stokes models for a fracture with nine contact areas. These correspond to $h = 0$ and 1 respectively. The Péclet number is unity in this figure, and the temperature profiles at $x = L$ are shown. The difference between the two profiles is small at small x-values and negligible for $Pe \geqslant 10$. Even at $Pe = 1$, the difference is small in the core of the fracture, and increases towards the walls. Since the Darcy model does not permit the no-slip condition at the sidewalls, the velocities in the x-direction tend to be larger here than in the Stokes model. Hence, the predicted temperature deviations from the mean are lower and the Darcy model computes the temperature field as better mixed. However, this difference is usually negligible and one may conclude

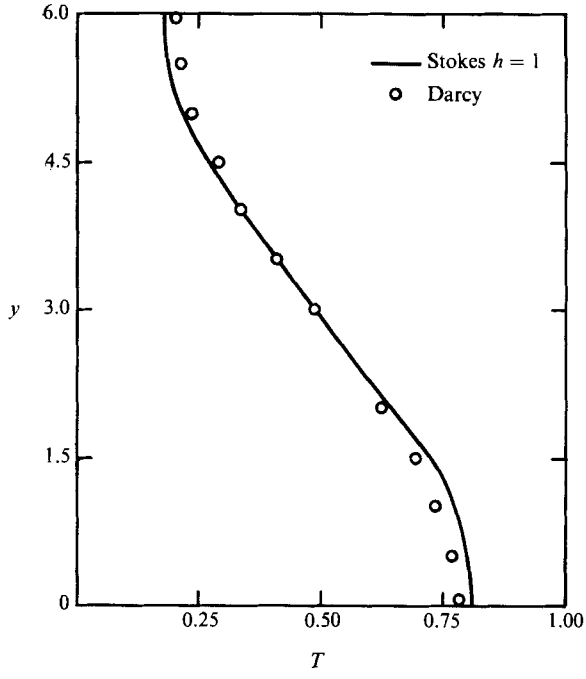

FIGURE 9. Comparison of temperature profiles in a fracture using Darcy and Stokes models; $Pe = 1$, $x = 6$, contact area 20%.

that the solution of the transport equation at a given Péclet number is insensitive to the choice of the flow model.

Further dispersion can occur in a fracture due to the complexity of flow path, as in a porous medium. Figures 10(*a*) and 10(*b*) show a comparison of temperature profiles at two Péclet numbers, in a fracture with and without contact areas. The contact area percentage is as high as 20%. The differences in the temperature profiles in the two figures are again seen to be small.

The results given above show that transverse dispersion is independent of (*a*) choice of aperture h and (*b*) the contact area percentage. It is a function only of Péclet number at steady state. For transport in a homogeneous, isotropic porous medium, $1/Pe$ is replaced by $(1/Pe+\gamma/d)$, where γ is the dispersion length (Dagan 1987) and d is the characteristic dimension appearing in the definition of Pe; γ is usually of the order of the pore size. The dispersion correction γ/d accounts for the complexity of the pore geometry in which the local flow occurs. It is seen in this study that such a correction is not necessary for fracture problems since the tortuosity of the flow path does not increase dispersion to any measurable extent.

4.2.2. *Unsteady flow and transport*

Under transient flow conditions, the total pressure drop which sustains flow will be larger than at steady state because part of the pressure drop goes towards accelerating the fluid. Transients arising from a jump in the magnitude of inlet flow are considered here. It is of interest to know the time taken by the fluid to reach steady state, and the influence of a distribution of contact areas in the fracture. Since the fluid is taken as incompressible, any change in mean velocity at the inflow boundary is instantaneously conveyed throughout the flow region. Transient effects

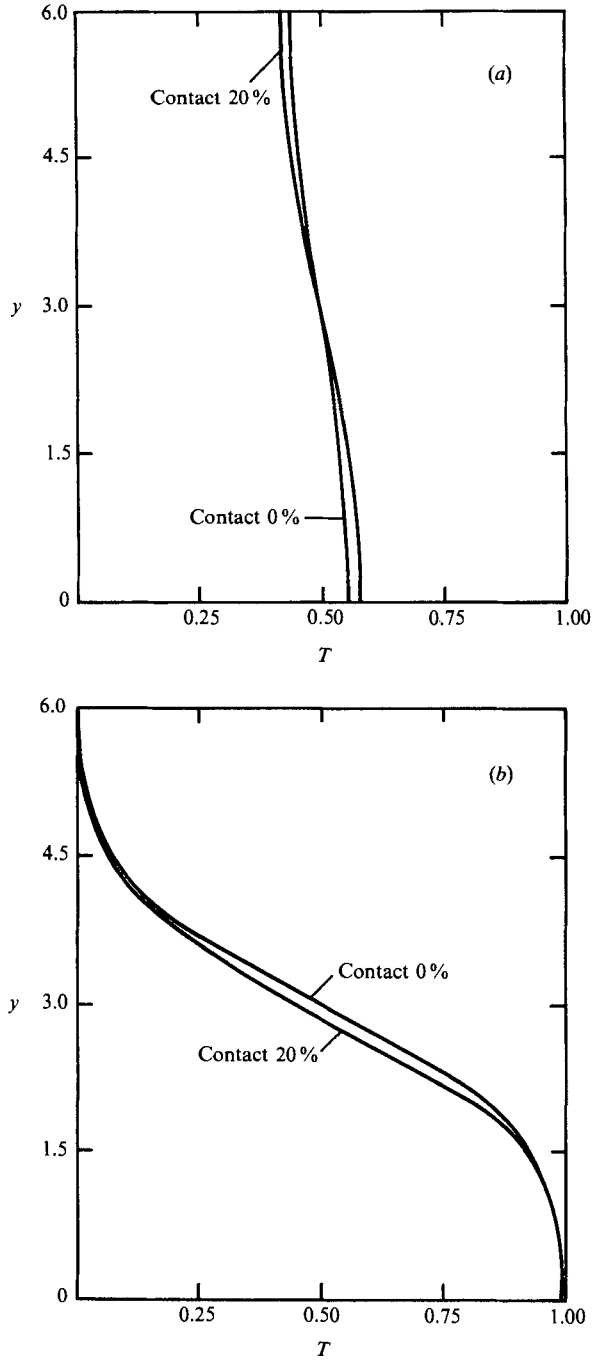

FIGURE 10. Comparison of temperature profiles in a fracture with and without contact areas, at $x = 6$: (*a*) $Pe = 0$; (*b*) $Pe = 10$.

are related to the time taken by the no-slip boundaries to make their presence felt on the increased flow rate. During this period, flow is accompanied by a large pressure drop and hence the equivalent permeability is smaller than the steady state value. The ratio of the instantaneous permeability to its steady-state value is called

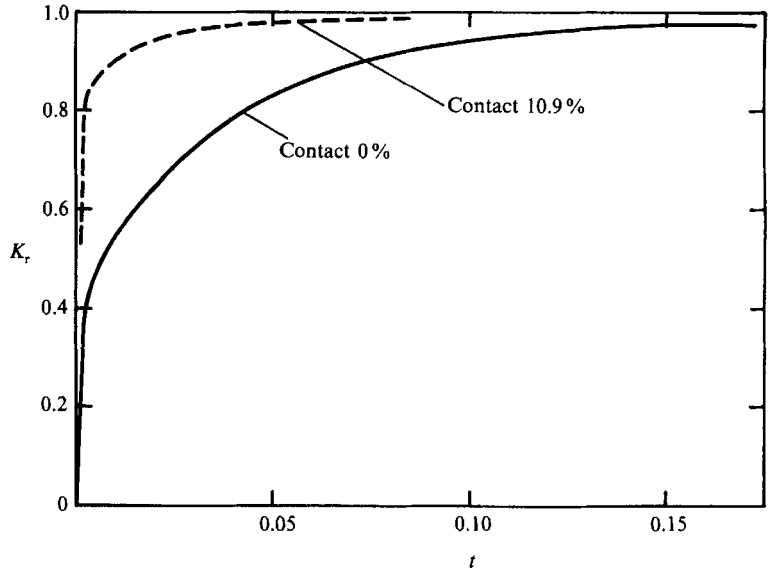

FIGURE 11. Relative permeability of a two-dimensional fracture as a function of time.

relative permeability K_r, in the present work. Figure 11 shows a plot of K_r as a function of dimensionless time for flow in a two-dimensional channel ($h \to \infty$), with no-slip sidewalls ($y = 0, L$), with and without contact areas.

Since transients exist in the presence of no-slip boundaries, a flow region with symmetry conditions applied to sidewalls and no contact area would respond instantaneously to changes in inlet flow. For a region with no-slip sidewalls, the diffusion of momentum will occur both along the flow direction and normal to it. This will lead to transients which will last for a time period proportional to L^2. The length of this time period is independent of the size of the jump in inflow. This has been confirmed by numerical experiments. Hence, the plots in figure 11 are applicable for all changes in mean velocity through the fracture, as long as Stokes flow conditions can be assumed to prevail in it. For a flow with contact areas, the average distance between solid boundaries is reduced, leading to an overall reduction in the transient period. The extent of this reduction depends on the fineness of distribution of contact area. In figure 11, the fracture is two-dimensional (i.e. $h \to \infty$) with five obstacles uniformly distributed over the flow domain. The average distance between solid boundaries is difficult to define but the ratio R = Flow area/Flow perimeter, is one way to measure it. When the contact area is 10.9% as in figure 11, R is 1.16. The transients last for a period of 0.15 units, when the contact area is zero. When the latter is 10.9%, the transients can be expected to last for $t = 0.15\,(R/L)^2 = 0.0056$ units. This is not precisely borne out in figure 11, but the drastic reduction in the unsteady period is clearly seen. For three-dimensional fractures, (finite h), the spacing between the top and bottom walls ($z = 0, h$) governs the diffusion time of transients. Hence, in fractures with small apertures, the flow may be assumed to reach steady state instantaneously.

It is assumed below that the flow is steady, and it is of interest to determine the rate of transport of thermal energy in a fracture, in an initially cold fluid. The transport equation contains h, the fracture aperture, only through the velocity components. However, the effect of including h has been shown to be small, in the

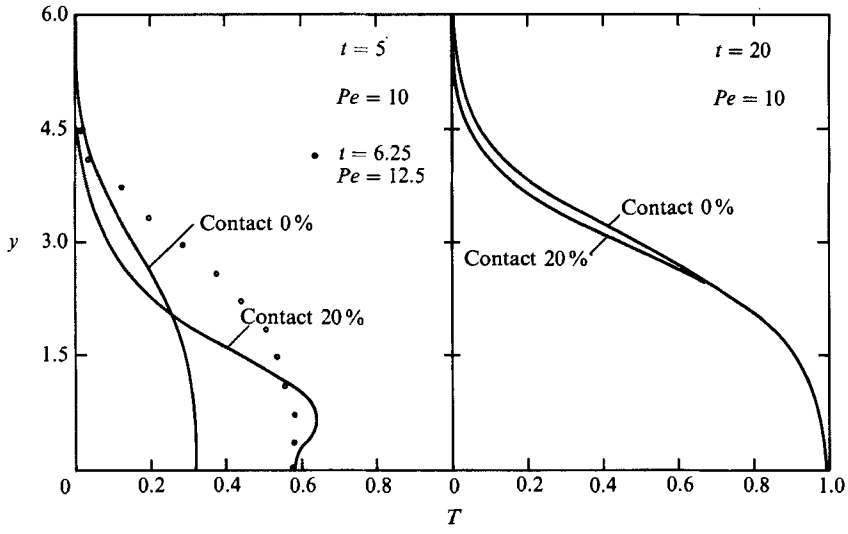

FIGURE 12. Unsteady transport in a fracture, with and without contact areas.

discussion on steady transport. This continues to hold for the unsteady problem as well. The velocity field corresponding to $h = 1$ has been used in the results reported below. Once again, the dispersion problem for the mixing of two streams at different temperatures is studied. Figure 12 shows temperature profiles at two different instants in a fracture, with and without contact areas. At $t = 5$ units, the temperature profiles at the fracture exit plane ($x = L$) are different for the fractures which have zero and 20 % contact. However, at $t = 20$ units, steady state is attained and the two profiles nearly merge. Hence, differences caused by a contact area distribution are important only if the transient period of transport is large.

It is clear from figure 12 that the transient temperature profile for a fracture with 20 % contact area resembles a high-Péclet-number solution, since the initial step profile continues to be preserved. To examine this point in greater detail, calculations have been performed here for transport of a uniform inlet temperature profile in a fracture, with and without contact areas. The results are shown in figures 13(a) and 13(b) for contact areas of 0 and 20 %, the latter coming from nine obstacles arranged in a uniform pattern. In the presence of contact areas, the exit temperature profile is not a constant. However, since the areas are evenly distributed over the fracture plane, the temperature at the mid-point ($x = L, y = \frac{1}{2}L$) is chosen as a representative or the most probable value on this plane. Results are given in figure 13(a, b) for Péclet numbers of 0.1, 1, 10 and 50. At $Pe = 0.1$, the difference in the results for $N = 0$ and 9 is insignificant. For $Pe = 10$ and 50, a front-type solution is seen for both $N = 0$ and 9. However, the front for $N = 9$ is located behind that of $N = 0$. At $Pe = 1$, the advection and diffusion mechanisms are of equal magnitude, and the difference between the profiles of $N = 0$ and 9 is not as small as at $Pe = 0.1$, nor as large as when $Pe = 10$ or 50. The solution for $Pe \to \infty$ and $N = 0$ is $T = 0, t < L$ and $T = 1, t > L$. This is a front at $t = L\,(= 6$, in this study). For $Pe = 10$ and 50 the temperature response is not as sharp as at $Pe \to \infty$, though it is centred at $t = 6$.

An explanation for the trends seen in figure 13(a, b) is as follows. At $Pe = 0.1$, the characteristic front velocity being governed by molecular diffusion is α/d. The time taken for the exit temperature to respond to an increase in the inflow temperature is Ld/α and primarily a function of the distance to be covered and the fluid

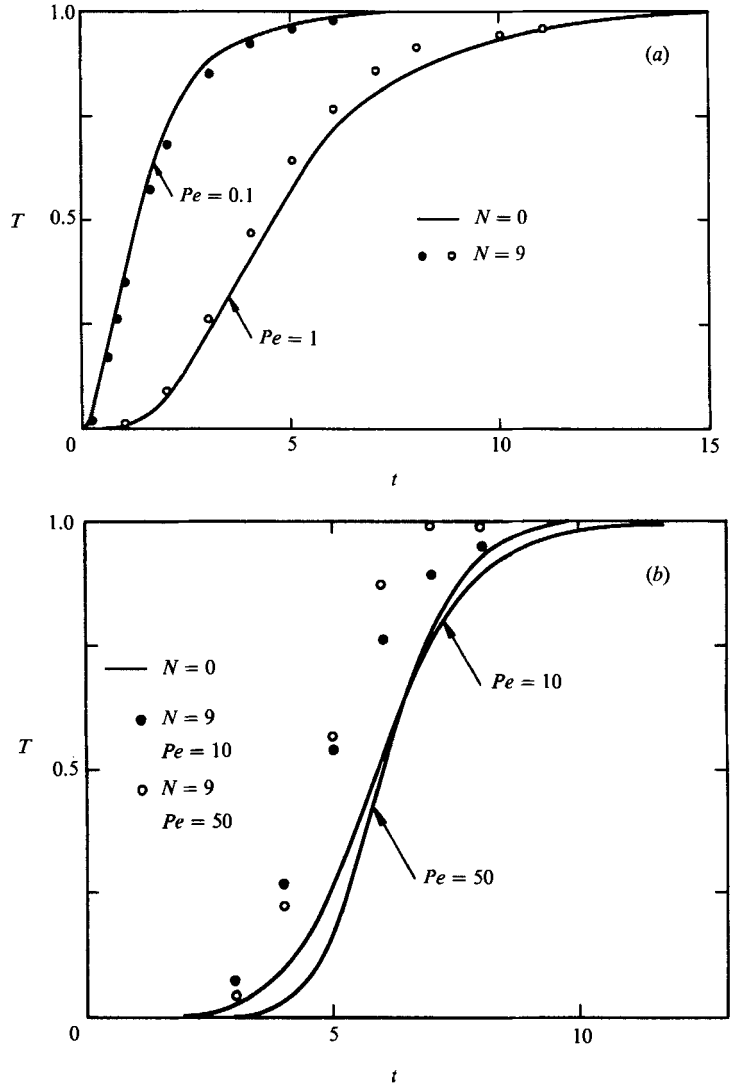

FIGURE 13. Rise in temperature at the exit plane of a fracture at $L = 6$: (*a*) $Pe = 0.1, 1$; (*b*) $Pe = 10, 50$.

diffusivity. Hence, at $Pe = 0.1$, the curves in figure 13(*a*) for $N = 0$ and 9 are nearly identical. At higher Péclet numbers ($Pe \geqslant 10$), the front velocity is close to the flow velocity in the fracture. For $N = 0$, this is u_m, the mean velocity at the inlet. For $N = 9$, the blockage due to contact areas increases the average velocity within the fracture. For a contact area fraction of C, this increase can be estimated as $1/(1-C)$. For $C = 0.2$, the average fluid velocity increases to $1.25u_m$. Hence, the thermal front will be seen not at $t = L$ but at $(1-C)L$, i.e. $0.8L$. This is 4.8 in the present problem. The fronts in figure 13(*b*), at $Pe = 10$ and 50, and $N = 9$ are indeed centred at $t = 4.8$, i.e. $T = 0.5$ at $t = 4.8$.

The simple correction for mean velocity to obtain the true dispersion profiles does not carry over to non-uniform thermal inflow conditions. For the mixing profile (14), figure 12 shows the corrected temperature values calculated in a parallel channel

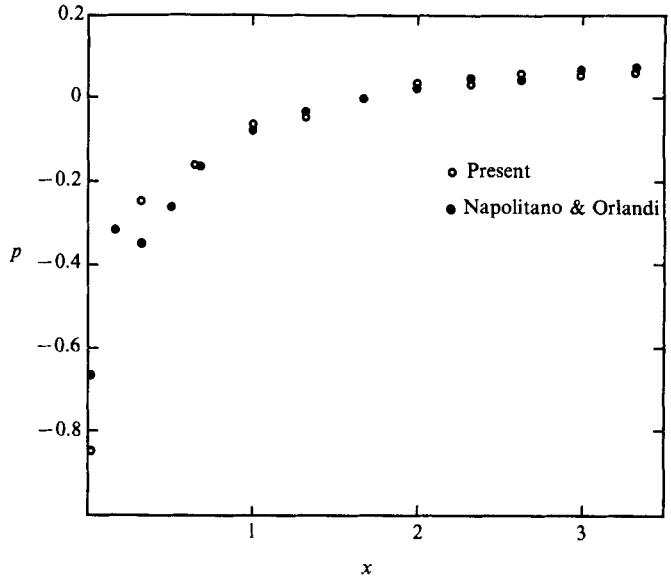

FIGURE 14. Comparison of computed wall pressure in an expanding channel with results of Napolitano & Orlandi (1985), $Re = 10$.

without contact areas. The correction has been carried out to account for 20% contact, i.e. the mean velocity is increased by a factor 1.25. This raises the Péclet number to 12.5 and time t non-dimensionalized by d/u_m to 6.25. Figure 12 shows that the correction is in the right direction, but is only qualitatively valid. Hence, we conclude that for an accurate simulation of dispersion, the governing equations must be solved in the complex flow space of the fracture.

5. Conclusions

Based on the model of a fracture as consisting of parallel plates with a distribution of contact areas, the following conclusions have been drawn in the present study.

(i) The equivalent permeability K of a fracture depends on both the aperture and the contact area. The Darcy model, with local permeability given as $h^2/12$, is applicable if $h/L \leqslant 0.016$, where L is the size of the smallest repeating pattern over the fracture plane. For $h/L \geqslant 0.016$, tortuosity effects are important and must be included in the permeability calculations. The depth-averaged Stokes equations can be used for this purpose.

(ii) The permeability K does depend on the pattern of distribution of contact area and the level of its fineness. However, the dependence becomes increasingly weak for small values of h. Further, for any h, K approaches a constant value as the fineness level is progressively increased.

(iii) In real fractures with sufficient contact area, flow transients last a very short time and hence can be ignored.

(iv) At steady state, the temperature distribution arising from the mixing of two streams is almost independent of the choice of the fracture aperture. It is also independent of the contact area fraction C for $C < 0.2$ and $Pe < 10$.

(v) Transient transport process can bring about significant changes in temperature profiles between fractures with zero and non-zero contact areas. The duration of the

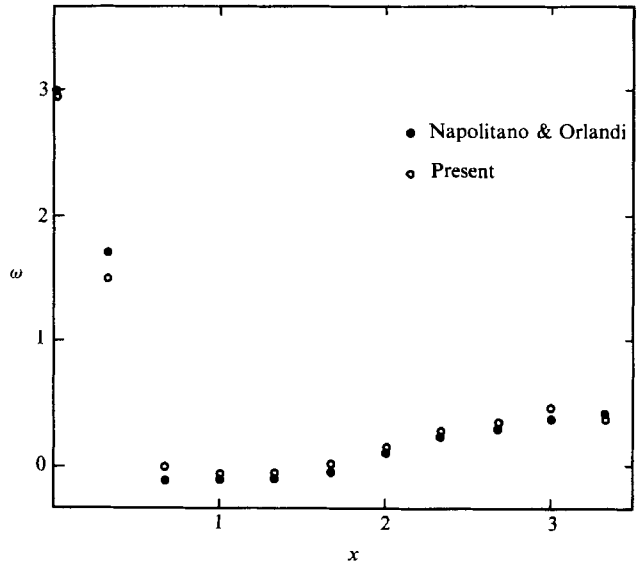

FIGURE 15. Comparison of computed wall vorticity in an expanding channel with Napolitano & Orlandi (1985), $Re = 10$.

transient is governed by the value of the Péclet number. For $Pe \leqslant 1$, transport is diffusion controlled and for $Pe \geqslant 10$, it is advection controlled. For a fracture with uniformly distributed contacts which occupy an area fraction C, the advection-controlled thermal front moves with an effective speed of $u_m/(1-C)$.

Part of flow calculations were carried out during the author's stay at Lawrence Berkeley Laboratory, USA. Remaining calculations were done on the ND-computer, CAD-project, IIT, Kanpur.

Appendix. Code validation

The computer code which solves Stokes equations is part of a larger program designed to solve Navier–Stokes equations in complex geometries. The latter has been extensively tested against several analytical solutions and published numerical solutions. In figure 14, the solution for wall pressure in an expanding channel is compared to the bench-mark result given by Napolitano & Orlandi (1985). In figure 15, the wall vorticity values are compared. Both comparisons are seen to be good. While these validate the Navier–Stokes code, only the Stokes part of it has been used in this work. The steady-state transport equation, $\boldsymbol{u}\cdot\nabla T = (1/Pe)\nabla^2 T$ has been solved for boundary conditions given by (14) in the text, and with no contact area. This equation is one-dimensional and has an analytical solution,

$$T(x,y) = \tfrac{1}{2} - \sum_{m=1}^{\infty} \frac{2}{(2m-1)\pi} \sin\frac{(2m-1)\pi}{2} \cos\frac{(2m-1)\pi y}{2} \exp\left(-\frac{(2m-1)^2\pi^2 x}{4Pe}\right). \tag{A 1}$$

The comparison between analytical and numerical solutions is shown in figure 16. The unsteady transport code has been tested against an analytical solution of a one-dimensional problem,

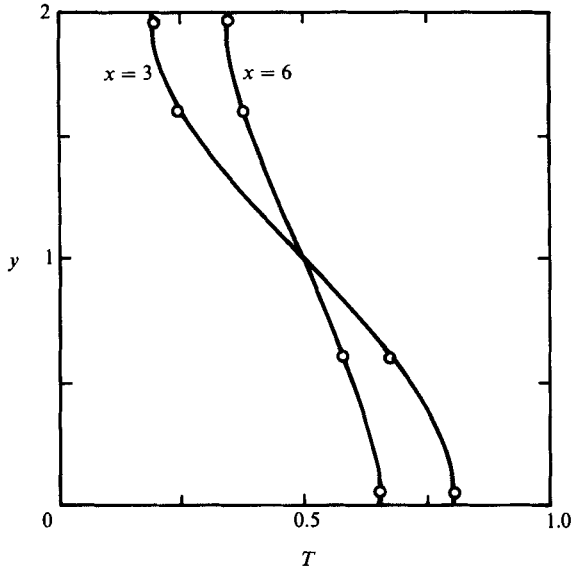

FIGURE 16. Comparison of numerical and analytical solutions for steady-state transport in a fracture, $Pe = 10$.

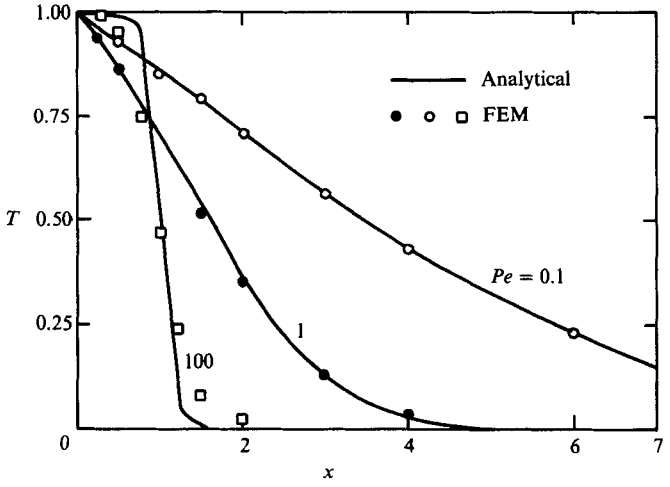

FIGURE 17. Comparison of numerical and analytical solutions for unsteady transport in a fracture at $t = 1$.

$$\left.\begin{aligned} T_t + T_x &= \frac{1}{Pe} T_{xx}, \\ t = 0, \quad T &= 0, \quad x > 0, \\ x = 0, \quad T &= 1, \quad t > 0, \\ x \to \infty, \quad T &= 0, \quad t > 0. \end{aligned}\right\} \tag{A 2}$$

This solution is

$$T(x,t) = \frac{2}{\pi^{\frac{1}{2}}} \int_{x/\left(\frac{4t}{Pe}\right)^{\frac{1}{2}}}^{\infty} e^{-\eta^2} \exp\left[Pe\left\{\frac{x}{2} - \frac{x^2}{16\eta^2} Pe\right\}\right] d\eta. \tag{A 3}$$

The comparison between the analytical and the unsteady numerical solutions is shown in figure 17.

REFERENCES

BAKER, A. J. 1983 *Finite Element Computational Fluid Mechanics*. McGraw-Hill.

BEAR, J. 1972 *Dynamics of Fluids in Porous Media*. Elsevier.

BROWN, S. R. 1987 Fluid flow through rock joints: the effect of surface roughness. *J. Geophys. Res.* **92**, 1337–1347.

CHAPMAN, N. A. & MCKINLEY, I. G. 1987 *The Geologic Disposal of Nuclear Waste*. John Wiley.

COULAUD, O., MOREL, P. & CALTAGIRONE, J. P. 1988 Numerical modelling of non-linear effects in laminar flow through a porous medium. *J. Fluid Mech.* **190**, 393–408.

DAGAN, G. 1987 Theory of solute transport by groundwater. *Ann. Rev. Fluid Mech.* **19**, 183–216.

DUFF, I. S. 1980 MA28 – A set of Fortran subroutines for sparse unsymmetric linear equations. AERE, Harwell.

KAYS, W. M. & CRAWFORD, M. E. 1980 *Convective Heat and Mass Transfer*. McGraw-Hill.

MONTAZER, P. & WILSON, W. E. 1984 Conceptual hydrologic model of flow in the unsaturated zone, Yucca Mountain, Nevada. *Water Resources Investigations Rep.* 84-4345. US Geological Survey.

NAPOLITANO, M. & ORLANDI, P. 1985 Laminar flow in a complex geometry: a comparison. *Intl J. Num. Methods Fluids* **5**, 667–683.

PATANKAR, S. V. 1980 *Numerical Heat Transfer*. Hemisphere.

PEYRET, R. & TAYLOR, T. D. 1983 *Computational Methods of Fluid Flow*. Springer.

PYRAK-NOLTE, L. J., MYER, L., COOK, N. G. W. & WITHERSPOON, P. A. 1987 Hydraulic and mechanical properties of natural fractures in low permeability rock. Presented at the *6th Inl Congr. on Rock Mechanics, Montreal, Canada*.

SCHLICHTING, H. 1979 *Boundary-Layer Theory*. McGraw-Hill.

SNOW, D. T. 1968 Rock fracture spacings, openings and porosities. *J. Soil Mech. Found. Div. Proc. ASCE* **94**, 73–91.

TSANG, Y. W. 1984 The effect of tortuosity on fluid flow through a single fracture. *Water Resources Res.* **20**, 1209–1215.

WALSH, J. B. & BRACE, W. F. 1984 The effect of pressure on porosity and transport properties of rocks. *J. Geophys. Res.* **89**, 9425–9431.

WANG, J. S. Y. & NARASIMHAN, T. N. 1985 Hydrologic mechanisms governing fluid flow in partially saturated, fractured porous tuff at Yucca Mountain. Prepared for Sandia Laboratories, Sandia Contract 47-7550. Also, *Water Resources Res.* **21**, 1861–1874.